Available online at www.sciencedirect.com
SCIENCE DIRECT®
Journal of Nuclear Materials 328 (2004) 225–231
journal of nuclear materials
www.elsevier.com/locate/jnucmat

Oxidation of the hexagonal $Zr(Cr_{0.4}Fe_{0.6})_2$ Laves phase

P.B. Bozzano [a], C. Ramos [b,1], F. Saporiti [b], P.A. Vázquez [b], R.A. Versaci [a], C. Saragovi [c,*]

[a] *Department of Materials, Centro Atomico Constituyentes (CAC), Comisión Nacional de Energía Atómica, Av. General Paz 1499 (1650), Buenos Aires, Argentina*
[b] *Instituto de Tecnología 'Prof. Jorge A.Sabato', UNSAM, Comisión Nacional de Energía Atómica, Av. General Paz 1499 (1650), Buenos Aires, Argentina*
[c] *Department of Physics, Centro Atomico Constituyentes (CAC), Comisión Nacional de Energía Atómica, Av. General Paz 1499 (1650), Buenos Aires, Argentina*

Received 2 September 2003; accepted 8 April 2004

Abstract

The hexagonal (C14-type) Laves phase $Zr(Cr_{0.40}Fe_{0.60})_2$ when oxidized in an open furnace was studied by X-ray diffraction and Mössbauer spectroscopy techniques. Oxidation modified part of the original Laves phase and Zr oxides, Cr oxides, α-Cr, (Fe, Cr) oxides, α-Fe and α-Fe_2O_3 appeared. The behaviour of these phases, particularly the Fe-bearing phases, is described in detail through a two stage process (stage I from 0 to ~7 wt% O_2 and stage II up to 22 wt% O_2). A very small amount of O_2 (stage I) is enough to induce the formation of α-Fe upon oxidation, sustaining a model previously suggested for the oxidation of the Laves phases. This α-Fe is highly Cr-substituted. Oxidation proceeds through the increasing presence of α-Fe_2O_3 and through the structural evolution of Zr oxides (formation of monoclinic, tetragonal and cubic ZrO_2).

1. Introduction

Oxidation of the Laves phase Zr(Cr, Fe)$_2$ is an important topic to study when considering Zircaloy-4 oxidation. As it is well known, Zircaloy-4 (Sn 1.45–1.5 wt%, Fe 0.18–0.24 wt%, Cr 0.07–0.13 wt%, O 1400 ppm and Zr to balance) is widely used as fuel cladding material in nuclear industry due to its low neutron-capture cross-section, high mechanical strength, high thermal conductivity and good corrosion resistance. Of all the alloying elements only Sn is in solid solution, and hence is relatively uniformly distributed. On the other hand, iron and chromium are essentially insoluble in Zr at low temperatures (<873 K) and they are, therefore, present almost entirely in the form of second phase particles [1]. There is only one intermetallic compound, Zr(Cr, Fe)$_2$, which occurs in two structural forms, hexagonal C14-type and cubic C15-type [2,3]. The proportions of cubic and hexagonal Zr(Cr, Fe)$_2$ present can be varied by different fabrication routes. Both types of precipitates are commonly present; usually the hexagonal variant is predominant. These intermetallic precipitates are about 10–1000 nm in diameter, depending on the fabrication conditions. The structure, composition, average size and morphology of the second phase precipitates are closely related to the corrosion behaviour of Zircaloy-4 [4–6].

Many studies were carried out in order to evaluate the evolution of the precipitates when Zircaloy-4 is oxidized [7–10]. Previous works [11,12] showed that precipitates undergo chemical composition changes after open

* Corresponding author. Tel.: +54-11 6772 7160; fax: +54-11 6772 7362.
E-mail address: saragovi@cnea.gov.ar (C. Saragovi).
[1] CONICET-Fundación YPF fellowship.

0022-3115/$ - see front matter © 2004 Elsevier B.V. All rights reserved.
doi:10.1016/j.jnucmat.2004.04.335

furnace oxidation: EDS (energy dispersive spectroscopy) studies detected the presence of Zr, Cr and Fe within both the non-oxidized and partially oxidized precipitates, but no Fe was detected within the oxidized ones. Then, it was suggested that a progressive Fe rejection towards the oxidized $Zr(Cr, Fe)_2$ precipitate/oxidized matrix frontier takes place. An empirical model has also been proposed for the Laves phase oxidation [13] stating that, at the beginning of the oxidation process at 923 K, Zr transforms to Zr_xO_{2-x}. The other elements, Cr and Fe remain in metallic state until the O partial pressure within the system increases up to a value high enough to allow the oxidation of Cr. The oxidized Cr diffuses first into the Zr_xO_{2-x} and then migrates to the surface. As oxidation proceeds, the O partial pressure increases up to a value high enough for the Fe contained in $Zr(Cr, Fe)_2$ to diffuse to the surrounding Zr_xO_{2-x}. EDS determinations pointed out a higher concentration of Cr on the external oxide surface '(Zr_xO_{2-x}, Cr_yO_{2-y})', and showed evidence of Fe atoms migration to an inner region than that of the oxidized – non-oxidized boundary.

The aim of this paper is to study the oxidation process of the hexagonal $Zr(Cr_{0.4}Fe_{0.6})_2$ Laves phase using Mössbauer spectroscopy (MS) complemented by X-ray diffraction (XRD) analysis for a further contribution to the mentioned experimental evidence.

At this point MS technique deserves a brief explanation seeing that, while it is not a commonly used technique in the conventional studies of zirconium alloys, our group has a vast experience in this subject [14–16]. The ^{57}Fe Mössbauer spectroscopy is a nuclear technique that provides information about the environments of the Mössbauer probe. This information is related to the electronic and magnetic properties of the Fe nuclei and their surroundings and it is provided by the hyperfine parameters. These parameters are the isomer shift (IS), the quadrupole splitting (QS) and the magnetic hyperfine field (H). The first one is mainly related to the oxidation state of the Fe ion, the second one to the symmetry of the charge distribution around the Fe nucleus and the last one, to the nature of the magnetic order around the probe. The knowledge of the characteristic hyperfine parameters allows the identification of a Fe-bearing phase, referring not only to a crystallographic phase but also to a magnetic and/or order–disorder phase. Furthermore, this technique allows the quantification of the identified Fe-bearing phases.

2. Experimental procedures

The Laves phase $Zr(Cr_{0.4}Fe_{0.6})_2$ (prepared from commercially Fe, Cr and Zr of nuclear purity) was arc melted with a non-consumable W electrode in an Ar atmosphere. A C14-type structure was determined by XRD analysis for the as-cast sample.

Table 1
Weight percent O_2 incorporated after oxidation process

Samples	A	B	C	D	E
wt% O_2	7.15	12.47	16.47	18.32	21.87

Then, the sample was powdered in an agate mortar and divided into five samples of about 2 mg. Each one was oxidized in an open furnace at 923 K during a short period of time in order to incorporate small amounts of O_2. The wt% of incorporated O_2 was evaluated by the weight gain using a Metler AE163 balance. The values so obtained are displayed in Table 1.

XRD analysis was performed on random powder samples in a Philips PW3710 diffractometer using Cu anticathode in a 22–120° range with an angle step of 0.02°. Due to the small amount of sample, the patterns were indexed using PDF data and comparing with spectra calculated using the Rietveld Structure Refinement software [17].

Mössbauer spectroscopy was performed at 300 K (RT: room temperature) in all the samples and in some of them also at 15 K. Absorbers were prepared in powder form, mixing with sugar to avoid texture effects [18]. The amount of powder used was calculated so that the thin approximation could be applied [19]. All the spectra were run at high velocity (11 mm/s); a low velocity (5 mm/s) was used when specified. Analysis of the spectra was carried out using a least-squares fitting program [20] and the goodness-of-fit of each fit was determined by χ^2 criteria. Doublets and sextets subspectra were used for sites and, where necessary, distributions of hyperfine fields were also used. Sites indicate similar ordered Fe environments whereas distributions of hyperfine fields indicate slightly different Fe environments. Subspectral areas were taken as a measure of Fe-bearing phase concentrations [21].

3. Results and discussion

3.1. X-ray diffraction analysis

Fig. 1 shows the XRD pattern obtained for the as-cast $Zr(Cr_{0.4}Fe_{0.6})_2$ powder sample. Hexagonal C14-type structure was found with the following lattice parameters: $a = 0.502 \pm 0.001$ nm, $c = 0.822 \pm 0.001$ nm.

Fig. 2 shows the XRD pattern for a characteristic oxidized powdered sample (sample D in this case). Table 2 displays the identified phases and the lattice parameters obtained for the oxidized samples.

According to the XRD results, other phases besides the C14-type one appeared upon oxidation: ZrO_2, α-Fe, α-Fe_2O_3, $(Cr, Fe)_2O_3$, without discarding the presence of α-Cr and α-Cr_2O_3 which were difficult to distinguish.

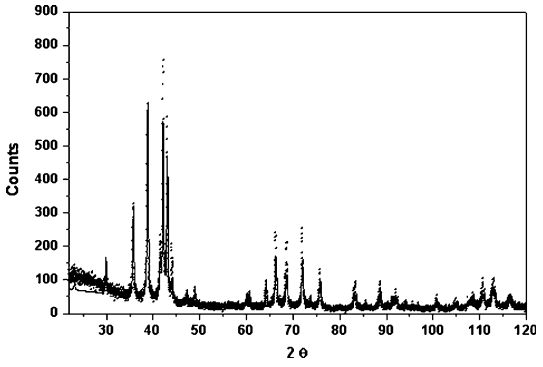

Fig. 1. XRD pattern for the as-cast (non-oxidized) $Zr(Cr_{0.4}Fe_{0.6})_2$ sample.

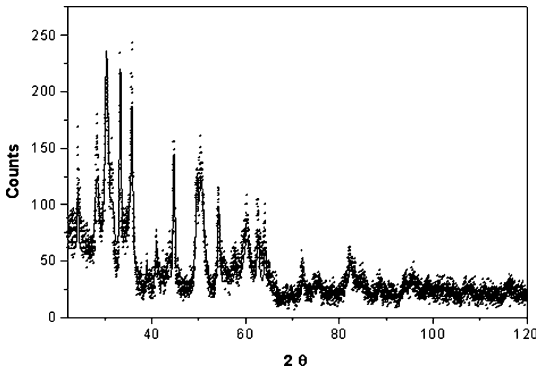

Fig. 2. XRD pattern for the $Zr(Cr_{0.4}Fe_{0.6})_2$ sample with 18.32 wt% O_2 (sample D).

The α-Cr reflections are almost coincident with the α-Fe ones and the same happens between α-Cr_2O_3, $(Cr, Fe)_2O_3$ and α-Fe_2O_3 reflections.

It is important to notice that the Zr oxides experience a structural evolution. Although the monoclinic structure is the stable one at temperatures bellow 1373 K, tetragonal and cubic structures were also detected. The monoclinic–tetragonal transformation has been found to take place at a much lower temperature and pressure than those expected from the phase diagram of pure microcrystalline zirconia. This result could be related to the nanostructure of the crystallites constituting oxidation scales [22]. Garvie [23] proposed that the tetragonal form, having a lower surface free energy than the monoclinic one, occurs spontaneously at a critical crystallite size at room temperature. The presence of cubic structure could be due to a strong stabilization effect. There is some consensus that Fe has a negligible solubility in monoclinic ZrO_2, up to 5 at.% in tetragonal ZrO_2 and up to 20 at.% in cubic ZrO_2, and if present at high concentrations stabilizes the higher symmetry phases [24]. In addition, chromium, some of which dissolved substitutionally in the ZrO_2 lattice, would play a major role in such stabilization [8,9].

3.2. Mössbauer spectroscopy analysis

The Mössbauer spectrum of the non-oxidized Laves phase sample run at 5 mm/s is shown in Fig. 3. It was fitted with two doublets, D1 and D2; the parameters obtained were coincident with those found in the literature [14,25,26]. Fig. 4 instead shows a characteristic feature of one of the oxidized samples spectra run at 11 mm/s (sample D). Oxidized samples spectra show complex shapes which were fitted by means of an 'average' doublet (D), one crystalline sextet (S1), two distributions of sextets (S2 and S3), and a singlet (s1).

The narrow S1 sextet with the broad S2 distribution were used to model the observed outer sharp sextet with

Table 2
Crystalline structure and lattice parameters obtained by XRD

Crystalline structure	Sample A (nm)	Sample B (nm)	Sample C (nm)	Sample D (nm)	Sample E (nm)	Proposed phases
Hexagonal C14-type	$a = 0.501$ $c = 0.820$	$a = 0.501$ $c = 0.821$	$a = 0.501$ $c = 0.821$	$a = 0.502$ $c = 0.822$	$a = 0.502$ $c = 0.821$	$Zr(Cr_{0.4}Fe_{0.6})_2$ Laves phase
Cubic I	$a = 0.287$	$a = 0.287$	$a = 0.290$	$a = 0.287$	$a = 0.289$	α-Fe, α-Cr
Hexagonal	–	$a = 0.503$ $c = 1.371$	$a = 0.503$ $c = 1.371$	$a = 0.503$ $c = 1.373$	$a = 0.502$ $c = 1.368$	Fe_2O_3, Cr_2O_3 $(Cr, Fe)_2O_3$
Monoclinic	$a = 0.515$ $b = 0.518$ $c = 0.532$	$a = 0.514$ $b = 0.518$ $c = 0.531$	$a = 0.514$ $b = 0.518$ $c = 0.532$	$a = 0.514$ $b = 0.518$ $c = 0.532$	$a = 0.513$ $b = 0.518$ $c = 0.531$	Monoclinic ZrO_2
Cubic F	–	$a = 0.510$	$a = 0.510$	$a = 0.510$	$a = 0.509$	Cubic ZrO_2
Tetragonal	$a = 0.359$ $c = 0.517$	$a = 0.360$ $c = 0.517$	$a = 0.359$ $c = 0.518$	$a = 0.359$ $c = 0.517$	$a = 0.359$ $c = 0.518$	Tetragonal ZrO_2

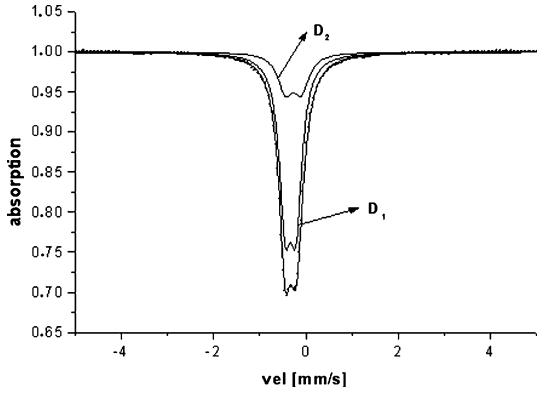

Fig. 3. Mössbauer spectrum of the non-oxidized $Zr(Cr_{0.4}Fe_{0.6})_2$ sample.

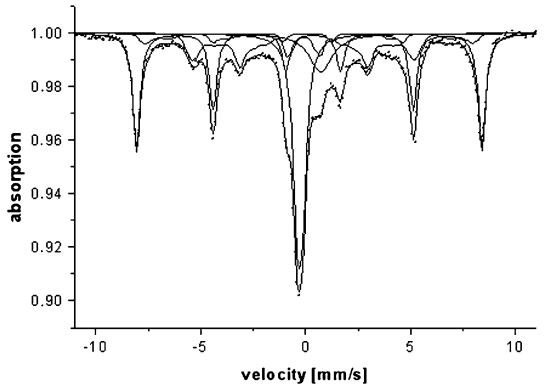

Fig. 4. Mössbauer spectrum of the $Zr(Cr_{0.4}Fe_{0.6})_2$ sample with 18.32 wt% O_2 (sample D).

Table 3
Mössbauer parameters at RT

Sample	FIT	IS (mm/s)	QS (mm/s)	H_M (T)
Non-oxidized	D1	−0.22	0.23	–
$Zr(Cr_{0.4}Fe_{0.6})_2$	D2	−0.16	0.34	–
A	S1	0.30	−0.24	51.34
	S2	0.11	−0.14	45.99
	S3	−0.02	−0.04	27.32
	D	−0.27	0.24	–
	s	0.32	–	–
B	S1	0.36	−0.23	51.13
	S2	0.40	−0.10	48.66
	S3	−0.01	0.05	28.54
	D	−0.20	0.24	–
	s	0.59	–	–
C	S1	0.36	−0.20	51.37
	S2	0.23	−0.02	47.04
	S3	0.00	−0.01	29.96
	D	−0.21	0.24	–
	s	0.72	–	–
D	S1	0.35	−0.19	51.17
	S2	0.21	0.06	46.69
	S3	−0.01	−0.01	30.03
	D	−0.21	0.25	–
	s	0.81	–	–
E	S1	0.33	−0.19	51.24
	S2	0.34	−0.19	48.57
	S3	−0.01	−0.03	27.9
	D	−0.21	0.25	–
	s	0.77	–	–

broad shoulders. The distribution of static hyperfine magnetic fields S3 reports instead the inner sextets. The resulting Mössbauer parameters at RT are summarized in Table 3. The values of the maxima of the distribution profiles are quoted as H_M. All the IS values are referred to that of α-Fe at RT.

The parameters corresponding to S1 allow assigning it to the presence of well crystallized hematite. On the other hand, the S2 distributions of lower hyperfine magnetic fields show slightly different environments around the Fe nuclei and points to a random Fe substitution by Cr into the hematite lattice. In the case of the sample with higher wt% of O_2, a spectrum was run at low temperature (15 K), its fit indicated that the Morin temperature did not occur which is coincident with Cr substitution by Fe. The fitted IS values are typical of Fe^{3+} environments.

S3 distributions take into account the rest of the magnetic signals although, in some of the oxidized samples, these spectra could also be fitted with a broad sextet ($\Gamma \approx 0.8$ mm/s). In both cases the parameters obtained are indicative of α-Fe presence but, because of S3 shapes, a further result is obtained which suggests that Cr atoms have been randomly introduced and perturbed an ordered α-Fe lattice. The fitted IS values are typical of metallic environments for the Fe ion.

Concerning the paramagnetic region and as it was already mentioned, the 'average' D doublet corresponds to the presence of the original Laves phase, $Zr(Cr_{0.4}Fe_{0.6})_2$. The singlet, s1, could correspond to the high velocity peak of a Fe^{3+} doublet in which the low velocity peak would be masked between the low velocity Laves phase signals. This singlet is assigned to the presence of $(Cr_x, Fe_y)_2O_3$ ($y < x$) [15].

Cr and Fe very similar atomic radii (0.1420 and 0.1411 nm respectively) apparently preclude noticing any substitution from one by each other. In fact the lattice parameters found are practically the same in all the series, suggesting no structural changes. A further result is provided by MS which shows a random Fe substitution by Cr in the hematite and in the α-Fe

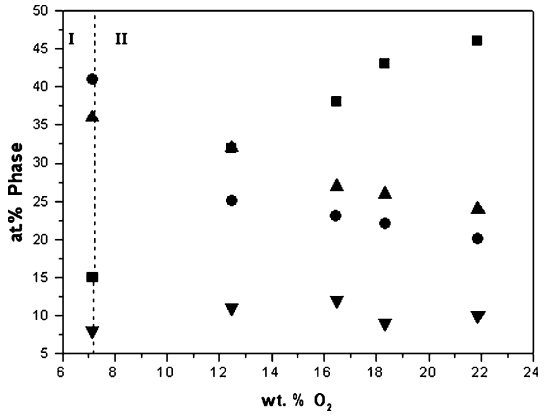

Fig. 5. Variation of the concentration of Fe-bearing phases with O_2 content. Notice that 0 wt% O_2 corresponds to the 100% non-oxidized Laves phase. ▼ α-$(Cr_x, Fe_y)_2O_3$, $(y < x)$; ■ α-Fe_2O_3; ▲ C14-type Laves phase; ● α-Fe.

lattices regarding the behaviour of the magnetic hyperfine fields.

Mössbauer results let to perform as well a semi-quantitative analysis of the Fe-bearing phases found by taking subspectral areas which are proportional to their concentration. Fig. 5 describes the variation of the concentration of each Fe-bearing phase with oxygen content based on these data which are normalized to 100%. Fig. 6 shows the concentrations of the 'crystalline' and the 'substituted' (Fe substituted by Cr into the phase lattice) contributions to the α-Fe_2O_3 and α-Fe subspectral areas respectively. This estimation was made considering S1 areas as 'crystalline' and S2 areas as 'substituted' contributions to the α-Fe_2O_3 phase. In return S3 subspectral area was divided into subareas which were respectively attributed to the 'crystalline' (BHF = 33 T) and the 'substituted' (remainder mean values of hyperfine field in the distribution profile) contributions to the α-Fe phase.

For a convenience matter Fig. 5 is divided into two zones: an O_2 low content zone (I) and a medium-high O_2 content zone (II). The first one shows that a low content introduction of O_2 (~7 wt%) induced the appearance of the expected α-Fe phase but also of the α-Fe_2O_3 phase. It would be necessary an even less O_2 content to allow the appearance of only α-Fe (among the Fe-bearing phases) at expenses of the Laves phase. It is interesting to notice that the α-Fe phase is present in the higher percentage amount and that it also presents the higher substituted to crystalline ratio (almost 2). After Zr and Cr oxidation, the remainder Cr preferred to substitute Fe in the metallic α-Fe lattice; the α-Fe_2O_3 and α-$(Cr_x, Fe_y)_2O_3$ $(y < x)$ phase concentrations are low and the substituted to crystalline ratio is almost 1 in the α-Fe_2O_3 phase.

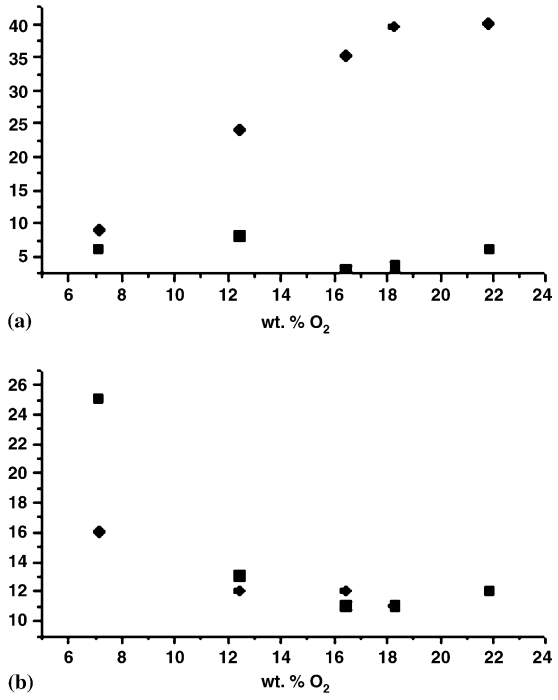

Fig. 6. 'Crystalline' (●) and 'substituted' (■) contributions to the α-Fe_2O_3 (a) and α-Fe (b) subspectral areas obtained by MS.

The second zone shows that a higher introduction of O_2 induces an increment of the α-Fe_2O_3 phase concentration while the Laves phase and the α-Fe concentrations decrease. This fact suggests that, at this stage, the oxidation process proceeds through the formation of α-Fe_2O_3 at expenses of the Laves phase and of the α-Fe phase. The remainder Cr, not occurring into Fe-bearing phases, stabilizes the cubic ZrO_2 phase and α-Cr_2O_3 and α-Cr would be formed in addition. Seeing that the Mössbauer probe used in this work is Fe, there is no Cr Mössbauer effect, thus this technique cannot confirm this hypothesis. Nevertheless it could be assumed that chromium is oxidized into fine Cr_2O_3 since the formation of Cr_2O_3 upon the oxidation of $ZrCr_2$ precipitates in a zirconium matrix has already been reported [27].

4. Conclusions

The structural and hyperfine properties of the Laves phase $Zr(Cr_{0.4}Fe0_{0.6})_2$ oxidized during short periods of time in open furnace are here presented; to our knowledge there are no reports from other groups on this subject. This Laves phase, present in the form of second phase particles in Zircaloy-4, plays an important role when considering Zircaloy-4 oxidation. In particular,

the redistribution of the alloying elements from the intermetallic particles into the oxide matrix has an important impact on the oxidation rate of the alloy, and to clarify this point it is essential to know which compounds are generated during the oxidation process.

Conclusions of the present work based on the isolated hexagonal Laves phase study may be summarized as:

- The introduction of O_2 produced a selective oxidation process, involving a structural evolution (formation of monoclinic, tetragonal and cubic zirconia) and a chemical evolution (iron/chromium depletion and oxidation). ZrO_2, α-Fe, α-Fe_2O_3 and the original C14 Laves phase were detected by XRD and/or MS, without discarding the presence of α-Cr and α-$(Cr, Fe)_2O_3$.
- The oxidation process cannot be accurately modelized by a simple parabolic law. It seems to proceed through two stages which were defined as stage I: from 0 to 7 wt%, and stage II: up to 22 wt% O_2.
  - In the first stage, monoclinic and tetragonal ZrO_2 were formed. Regarding the Fe-bearing phases, the expected α-Fe phase is noteworthy present (almost 42% in Fig. 5) with a highly degree of Fe substitution by Cr. This Cr probably comes from the remaining non-oxidized Cr. However α-Fe_2O_3 with a slight Cr substitution and α-$(Cr_x, Fe_y)_2O_3$ ($y < x$) also appeared, eventhough in a small amount. It is a difficult task, from an experimental point of view, to incorporate a less amount of O_2 to complete the intermediate points of stage I.
  - In the second stage, the oxidation proceeds through the increment of α-$(Cr, Fe)_2O_3$. The cubic ZrO_2 phase stabilizes and α-Cr_2O_3 and α-Cr would develop.
- Finally, it can be mentioned that although Mössbauer Spectroscopy is not a commonly used technique in the conventional studies of zirconium alloys, it was demonstrated here that it is particularly suited to investigate the oxidation process of Fe-bearing phases.

Acknowledgements

We gratefully acknowledge Dr Maria Ortiz for helpful discussions on XRD study and A. Carnero for technical assistance.

References

[1] D. Charquet, R. Hahn, E. Ortlieb, J.P. Gros, J.F. Wadier, in: Proceedings of the 8th International Symposium on Zirconium in the Nuclear Industry, ASTM-STP 1023, Philadelphia, 1988, p. 405.
[2] R.A. Versaci, M. Ipohorski, J. Nucl. Mater. 80 (1979) 180; R.A. Versaci, M. Ipohorski, J. Nucl. Mater. 116 (1983) 321.
[3] X.Y. Meng, D.O. Northwood, J. Nucl. Mater. 137 (1986) 217.
[4] P. Rudling, K.L. Vannsesjö, G. Vesterlund, A.R. Massih, in: Proceedings of the 7th International Symposium on Zirconium in the Nuclear Industry, ASTM-STP 939, Philadelphia, 1987, p. 292.
[5] H.G. Weidinger, H. Ruhmann, G. Cheliotis, M. Maguire, T.L. Yau, in: Proceedings of the 9th International Symposium on Zirconium in the Nuclear Industry, ASTM-STP 1132, Philadelphia, 1991, p. 499.
[6] D.G. Franklin, P.M. Lang, in: Proceedings of the 9th International Symposium on Zirconium in the Nuclear Industry, ASTM-STP 1132, Philadelphia, 1991, p. 3.
[7] T. Kubo, M. Uno, in: Proceedings of the 9th International Symposium on Zirconium in the Nuclear Industry, ASTM-STP 1132, Philadelphia, 1991, p. 476.
[8] D. Pêcheur, F. Lefebvre, A. Motta, C. Lemaignan, J.F. Wadier, J. Nucl. Mater. 189 (1992) 318.
[9] D. Pêcheur, F. Lefebvre, A. Motta, C. Lemaignan, D. Charquet, in: Proceedings of the 10th International Symposium on Zirconium in the Nuclear Industry, ASTM-STP 1245, Philadelphia, 1994, p. 687.
[10] X. Iltis, F. Lefebvre, C. Lemagnan, J. Nucl. Mater. 224 (1995) 121.
[11] P.B. Bozzano, M. Ipohorski, R.A. Versaci, Acta Microscopica 5 (B) (1996) 238.
[12] R. A. Versaci, P.B. Bozzano, M. Ipohorski, in: Proceedings of the Conference on Materials and Nuclear Power. EUROMAT 96, Bournemouth, UK, 1996, p. 411.
[13] P.B. Bozzano, M. Ipohorski, R.A. Versaci, in: Proceedings of the Electron Microscopy Symposium ICEM 14, 1998, p. 105.
[14] F. Labenski de Kanter, C. Saragovi, M. Granovsky, D. Arias, in: E. Baggio-Saitovich, E. Galvao da Silva, H.R. Rechenberg (Eds.), Applications of the Mössbauer Effect, World Scientific, Singapore, 1992, p. 246.
[15] F. Saporiti, P. Bozzano, R. Versaci, C. Ramos, P. Vázquez, I. Raspini, C. Saragovi, Hyperfine Interact. 139&140 (2002) 379.
[16] P. Bozzano, P. Vázquez, F. Saporiti, C. Ramos, R. Versaci, C. Saragovi, Hyperfine Interact. C 5 (2003) 519.
[17] L. Lutterotti, P. Scardi, J. Appl. Crystallogr. 25 (1992) 459.
[18] T. Ericsson, R. Wäppling, J. Phys. 6 (1976) 719.
[19] G.J. Long, T.E. Cranshaw, G. Longworth, Mössbauer Effect Data Ref. J. 6 (2) (1983) 42.
[20] R.A. Brand, NORMOS program, Int. Rep. Angewandte Physik, Univ. Duisburg (1990).
[21] A.H. Muir, New York, Analysis of complex Mössbauer spectra by stripping techniques in IJ Gruverman ed Mössbauer Effect Methodology, vol. 4, Plenum, 1968, p. 75.
[22] P. Bouvier, J. Godlewski, G. Lucazeau, J. Nucl. Mater. 300 (2002) 118.
[23] R.C. Garvie, J. Phys. Chem. 69 (1965) 1238; R.C. Garvie, J. Phys. Chem. 82 (1978) 218.

[24] S. Davison, R. Kerrshaw, K. Dwight, A. Wold, J. Solid State Chem. 73 (1988) 47.
[25] J.A.H. Coaquira, H.R. Rechenberg, J. Mestnik Filho, A.W. Carbonari, J. Alloys Compd. 356&357 (2003) 200.
[26] J.A.H. Coaquira, H.R. Rechenberg, J. Mestnik Filho, J. Alloys Compd. 288 (1999) 42.
[27] B. De Gelas, G. Beranger, P. Lacombe, J. Nucl. Mater. 28 (1968) 185.